

A Determination of the Molecular Parameters for NiH in Its ${}^2\Delta$ Ground State by Laser Magnetic Resonance¹

THOMAS NELIS²

*Institut für Angewandte Physik der Universität Bonn, Wegelerstrasse 8, D5300, Bonn 1,
Federal Republic of Germany*

STUART P. BEATON³ AND KENNETH M. EVENSON

Time and Frequency Division, NIST, Boulder, Colorado 80303

AND

JOHN M. BROWN

Physical Chemistry Laboratory, South Parks Road, Oxford OX1 3QZ, England

The rotational spectrum of the NiH radical in the $v = 0$ level of its $X^2\Delta$ state has been studied by laser magnetic resonance (LMR) at far-infrared wavelengths. Transitions have been detected for all five isotopes of nickel and within both the lower (${}^2\Delta_{5/2}$) and upper (${}^2\Delta_{3/2}$) spin components. Nuclear hyperfine splittings for both the proton and ${}^{61}\text{Ni}$ ($I = \frac{3}{2}$) are observed. The effective Zeeman Hamiltonian for a molecule in a ${}^{2S+1}\Delta$ state is developed and used to fit all the available data for NiH in the $v = 0$ level. This includes the magnetic resonance observations of the (1,0) vibration-rotation band and the fine structure transitions in the $v = 0$ level (also by LMR) and the lambda-doubling intervals for the ${}^2\Delta_{3/2}$ component. There are several indications that this exercise is only just possible in the case of NiH in its $X^2\Delta$ state. The results are used to determine the equilibrium bond length of NiH, $r_e = 0.14694493(63)$ nm. © 1991 Academic Press, Inc.

1. INTRODUCTION

The transition metal hydride NiH is of interest for several reasons. Its bonding is relevant to a description of heterogeneous catalysis (1) and the dissociation of hydrogen on Ni surfaces (2). It is also of some astrophysical interest, having been identified in the sunspot spectrum (3). Finally, it provides a particularly demanding test for ab initio calculations because of the strong electron correlation effects in the 3d shell of the Ni atom. Reliable calculations of the transition metal hydrides have only recently become available (4–8). There has been a healthy interaction between theoreticians and experimentalists in this field. The calculations are guided and constrained by the experimental results while the execution and interpretation of experiments are often greatly aided by theoretical predictions.

¹ Supported in part by NASA Contract W, 15-047.

² Present address: Laboratoire Aimé Cotton, Campus d'Orsay, 91405 Orsay, France.

³ Present address: Department of Chemistry, University of Denver, Denver CO 80208.

The molecule NiH was first identified in 1934 by Gaydon and Pearse, who observed two strong band systems in the red and orange regions of the optical spectrum (9, 10). These observations were made by focusing the emission from a flame containing Ni(CO)₄ onto the slit of a grating spectrograph. The two band systems were subsequently designated $A^2\Delta_{5/2}-X^2\Delta_{5/2}$ and $B^2\Delta_{5/2}-X^2\Delta_{5/2}$. A few years later, Heimer photographed the same spectrum in absorption and discovered another band system at violet wavelengths (11), which is also a $^2\Delta_{5/2}-^2\Delta_{5/2}$ transition labeled $C-X$. When Åslund *et al.* rephotographed the violet system of NiH in 1964, they discovered the $C^2\Delta_{3/2}-X^2\Delta_{3/2}$ transition and also the weaker $C^2\Delta_{3/2}-X^2\Delta_{5/2}$ transition (12). This enabled the large spin-orbit splitting of 1015 cm⁻¹ in the ground state to be determined for the first time. In 1972, Smith (13) published electronic spectra of several transition metal hydrides which he generated by heating the appropriate metal powder in a mixture of hydrogen and argon in a shock tube. In addition to the known band systems of NiH in the red and orange regions, he discovered two new systems, one in the green and the other in the ultraviolet. He was unable to analyze these bands because they were heavily perturbed. More detailed analysis of the various band systems of NiH and NiD has been carried out by Scullman and co-workers (14, 15). In the later paper, they identified eight separate electronic states of NiH.

In more recent years spectroscopic experiments have been performed on NiH using lasers instead of grating spectrographs. Stevens Miller *et al.* (16) have recorded the laser photoelectron spectrum of NiH⁻. In these experiments, they were able to measure the energies of some low-lying electronic states of NiH relative to the ground $^2\Delta$ state although they could not identify them unambiguously. Field and his co-workers have recorded lines in the orange ($B-X$) system of NiH by laser excitation spectroscopy (17-20). In their experiments, NiH molecules were formed by sputtering Ni in the presence of H₂ and expanding the resultant gases into a low vacuum region, thereby effecting some cooling of the molecules. They have observed both Stark (17) and Zeeman effects (18, 20) and used these results to aid their assignment of the electronic states. Kadavathu *et al.* have recently observed transitions from the excited B state of NiH back down to vibrational levels of its low-lying $^2\Pi$ and $^2\Sigma$ states and firmly established the location of these states for the first time (21). By forming NiH inside the cavity of a dye laser, Hill and Field (22) have been able to saturate absorption lines in the optical spectrum. The linewidths obtained were sub-Doppler, sufficiently narrow to permit the resolution of ⁶¹Ni hyperfine structure.

Observations have also been made on the infrared spectrum of NiH. The first measurement of the ground state vibrational interval was made by Wright *et al.* in a matrix (23). The same transition has recently been detected in the gas phase by Nelis *et al.* (24) using carbon monoxide laser magnetic resonance (LMR). Only transitions within the lower, $^2\Delta_{5/2}$ spin manifold could be detected in these experiments. Very recently, Lipus *et al.* (25) have succeeded in detecting transitions in the 10 μm region between the two fine structure components of NiH by carbon dioxide laser magnetic resonance. These observations provide a more accurate measurement of the spin-orbit coupling constant. Finally, lambda-doubling transitions in the $^2\Delta_{3/2}$ spin component have been observed by Steimle *et al.* (26) by the technique of microwave optical double resonance.

We have already published a preliminary communication reporting the detection of pure rotational transitions in the ${}^2\Delta_{5/2}$ state of NiH by far-infrared LMR (27). This paper is concerned with a full description of the observations and their analysis. The observations have been extended to include transitions within the ${}^2\Delta_{3/2}$ component. Transitions involving all five naturally occurring isotopes of Ni have been observed (the least abundant isotope is ${}^{64}\text{Ni}$ at 1.08%). The majority of the resonances show a small doubling which arises from the proton hyperfine structure. In addition, a few transitions of ${}^{61}\text{NiH}$ have been detected which show the quartet hyperfine pattern expected for a nucleus with $I = \frac{3}{2}$. The data are fitted to within experimental uncertainty by a suitable effective Hamiltonian. New terms have been developed to describe the effect of the external magnetic field on a molecule in a ${}^2\Delta$ state. The structural implications of the parameters determined in the fit are discussed. A table of the frequencies of the pure rotational transitions of NiH in its ground state is given to aid the search for the molecule in astrophysical sources.

2. EXPERIMENTAL DETAILS

The spectra were recorded in the laboratories of the National Institute of Standards and Technology, Boulder, Colorado using an optically pumped far-infrared laser magnetic resonance spectrometer which has been described in detail elsewhere (28). The uncertainty in the laser frequency was about 0.5 MHz. The magnetic field could be scanned from 0 to 2 T. It was calibrated from time to time against a proton magnetic resonance fluxmeter. The accuracy of measurement was 10^{-5} T below 0.1 T and $10^{-4} B_0$ above this value.

The NiH radicals were generated in the spectrometer sample volume by the reaction of hydrogen atoms with nickel tetracarbonyl. The H atoms were produced by passing H_2 in He (at partial pressures of 13 and 270 Pa, respectively) through a microwave discharge running at about 50 W. Only a trace of $\text{Ni}(\text{CO})_4$ was required to form the NiH, corresponding to a partial pressure of about 0.25 Pa. Under these conditions, there was a dull, deep red flame in the region where the carbonyl was injected into

TABLE I

Summary of Transitions Observed in NiH in the $v = 0$ Level of the $X^2\Delta$ State by Far-Infrared LMR

Spin component	Transition $J' \leftarrow J''$	Laser Line		Lasing gas
		$\lambda/\mu\text{m}$	ν/MHz^a	
${}^2\Delta_{5/2}$	$7/2 \leftarrow 5/2$	186.0	1 611 421.9	CH_3OH
		183.6	1 632 666.9	CH_2DOH
	$11/2 \leftarrow 9/2$	118.8	2 522 781.6	CH_3OH
${}^2\Delta_{3/2}$	$5/2 \leftarrow 3/2$	256.0	1 170 941.0	CH_2F_2
	$7/2 \leftarrow 5/2$	183.6	1 632 666.9	CH_2DOH

^a Laser frequencies taken from the review by Inguscio, et al. (29)

the stream of atoms. An increase in the carbonyl partial pressure caused a sharp reduction in the signal, although the red flame became slightly stronger. Attempts to generate NiH by passing both H_2 and $Ni(CO)_4$ through the discharge were unsuccessful and produced only a heavy deposit of nickel (presumably).

3. DESCRIPTION OF THE FAR-INFRARED LMR SPECTRUM

Four rotational transitions of NiH in its $X^2\Delta$ state, two in the $^2\Delta_{5/2}$ and two in the $^2\Delta_{3/2}$ spin component, have been detected in the present study. The results are summarized in Table I, together with the details of the laser lines used. They are also shown in the energy level diagram in Fig. 1. In total, 327 resonances have been observed. As an example, the LMR spectrum associated with the $R(\frac{5}{2})$ transition in both spin

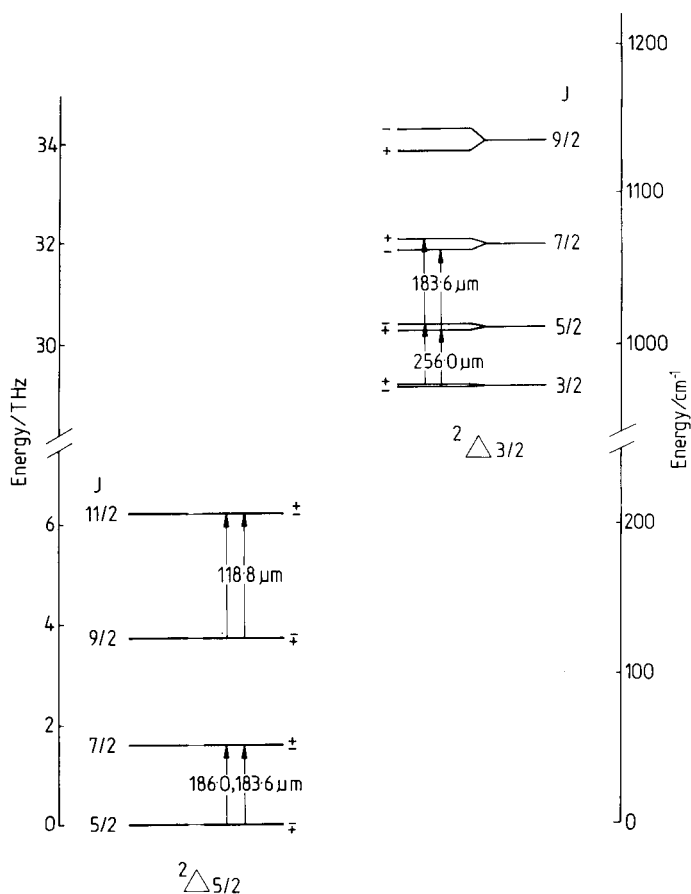


FIG. 1. Diagram showing the lower rotational levels of the NiH radical in the two spin components of its ground $^2\Delta$ state. The transitions detected in the far-infrared LMR spectrum are indicated. The Λ -type (parity) doubling has been exaggerated by a factor of 20 for clarity. Even on this scale the doubling for the levels in the $^2\Delta_{5/2}$ component is not discernible.

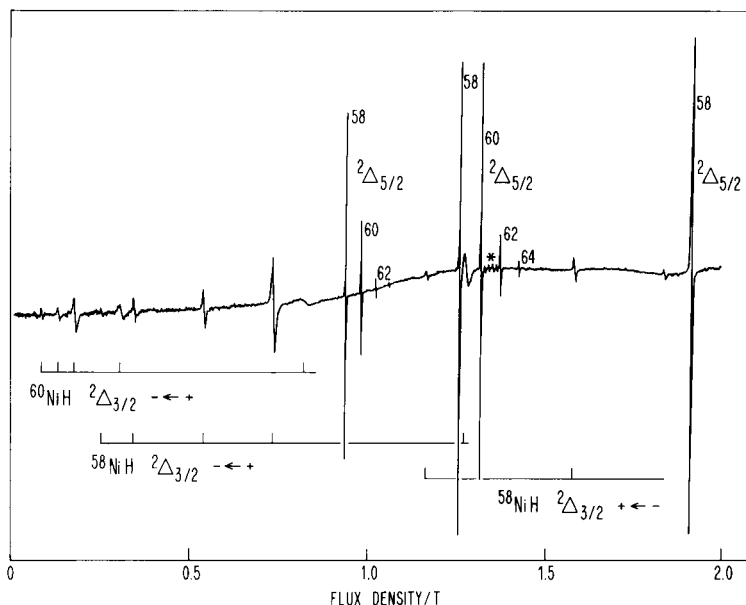


FIG. 2. Part of the far-infrared laser magnetic resonance spectrum of the NiH radical in the $v = 0$ levels of its $X^2\Delta$ state. The spectrum was recorded with the 183.6- μm line of CH_2DOH in σ (perpendicular) polarization so that the transitions obey the selection rule $\Delta M_J = \pm 1$. Zeeman components of the $J = 3\frac{1}{2} \leftarrow 2\frac{1}{2}$ rotational transition in both upper ($^2\Delta_{3/2}$) and lower ($^2\Delta_{5/2}$) spin components can be identified. For the stronger transitions, in the $^2\Delta_{5/2}$ component, resonances for all possible isotopic forms of NiH can be seen. The weak quartet for ^{61}NiH at about 1.3 T, marked with an asterisk, arises from the ^{61}Ni hyperfine structure ($I = \frac{3}{2}$).

components is shown in Fig. 2. The spectrum was recorded using the laser line of CH_2DOH at 183.6 μm in perpendicular (σ) polarization. The signal-to-noise ratio of 500:1 with $RC = 300$ msec is a convincing demonstration of the sensitivity of the far-infrared LMR technique. In fact, the sensitivity is high enough to permit the observation of all five stable nickel isotopomers (^{58}Ni 67.9%, ^{60}Ni 26.2%, ^{61}Ni 1.2%, ^{62}Ni 3.7%, ^{64}Ni 1.1%). Even the hyperfine quartet of ^{61}Ni ($I = \frac{3}{2}$) can be seen in Fig. 1 despite its low natural abundance.

Figure 2 shows transitions for both spin components recorded on a single scan. The transitions for the $^2\Delta_{5/2}$ component are much stronger because the $^2\Delta_{3/2}$ component is about 1015 cm^{-1} higher in energy. By measuring the observed signal strength and modifying it by the calculated transition probability, we estimate a population of the $^2\Delta_{3/2}$ state of 1.7% relative to the $^2\Delta_{5/2}$ state. This corresponds to a sample temperature of 350 K, slightly above room temperature. Although not obvious in Fig. 2, almost all resonances show a small doubling arising from the proton hyperfine structure. In addition, the $^2\Delta_{5/2}$ lines show a further doubling of similar magnitude which is the effect of lambda-type doubling. The lambda doubling of the $^2\Delta_{3/2}$ levels is much larger, giving two distinct Zeeman patterns separated by several hundred milliteslas as can be seen in Fig. 2.

4. ANALYSIS OF THE SPECTRUM

(i) *Quantum Number Assignments*

Because the angular momenta of NiH are coupled essentially in accordance with the Hund's case (a) scheme for the levels involved in this work, the Zeeman effect is very nearly linear in flux density. Consequently, the Zeeman patterns are quite characteristic and, combined with the known abundances of the nickel isotopes, lead directly to the quantum number assignments. The details of the observed resonances together with the assignments are given in Table II for all Ni isotopes with $I = 0$ and in Table III for ^{61}NiH (^{61}Ni has a spin of $\frac{3}{2}$).

(ii) *The Effective Hamiltonian*

The effective Hamiltonian can be considered in three parts, the zero field terms describing the spin and rotational levels, the nuclear hyperfine structure Hamiltonian, and the Zeeman Hamiltonian describing the effect of the applied magnetic field. The first operator is quite standard and has been described in detail by Brown *et al.* (30). With the addition of the lambda-doubling terms for a Δ state given by Brown *et al.* (31), the effective Hamiltonian is

$$\begin{aligned}
 H_{\text{eff}} = & BN^2 - DN^4 + AL_zS_z + \frac{2}{3}\lambda(3S_z^2 - S^2) + (\gamma + \gamma_D N^2)N \cdot S \\
 & + \frac{1}{2}q_\Delta(J_+^4 + J_-^4) - \frac{1}{2}(p_\Delta + 4q_\Delta)(J_+^3S_+ + J_-^3S_-) \\
 & + \frac{1}{2}(o_\Delta + 3p_\Delta + 6q_\Delta)(J_+^2S_+^2 + J_-^2S_-^2) - \frac{1}{2}(n_\Delta + 2o_\Delta + 3p_\Delta + 4q_\Delta) \\
 & \quad \times (J_+S_+^3 + J_-S_-^3) + \frac{1}{2}(m_\Delta + n_\Delta + o_\Delta + p_\Delta + q_\Delta)(S_+^4 + S_-^4). \quad (1)
 \end{aligned}$$

The explicit matrix elements for a molecule in a $^2\Delta$ state are given in Hund's case (a) basis set in Ref. (31). The different isotopic forms of NiH have been fitted simultaneously to the effective Hamiltonian in Eq. (1), using the appropriate isotopic scaling factors for the different parameters (30). This procedure worked well for all the parameters apart from the equilibrium rotational constant B_e (which is the primary parameter determined by the far-infrared data) and the spin-orbit coupling constant A_e (determined by the 10- μm data). For B_e , it was necessary to take account of non-adiabatic effects as described by Watson (32) and to scale the parameter as

$$\mu^{-1} \left[1 + \frac{m_e}{m_{\text{Ni}}} \Delta_{01}(\text{Ni}) + \frac{m_e}{m_{\text{H}}} \Delta_{01}(\text{H}) \right], \quad (2)$$

where μ is the reduced mass of the diatomic molecule, m_e is the mass of the electron, and m_{Ni} and m_{H} are the masses of the Ni and H atoms, respectively. For A_e , we introduced a mass dependence of a similar form as Eq. (2) except that the factor outside the brackets is μ^0 . The Born-Oppenheimer correction factor is referred to as $\Delta_{0,i}(\text{Ni})$ in this case. In the final stages of the fit of the data described below in Section (iv), we introduced a similar Born-Oppenheimer correction to the isotopic scaling of the spin-rotation constant, γ . This correction, designated $\Delta_{0,\gamma}(\text{Ni})$, was introduced in the form of Eq. (2) and made allowance for the different isotopic dependence of the rotational constant for the two spin components.

TABLE II
Transitions in the Far-Infrared LMR Spectrum of NiH

M_J	M_I	Parity	^{58}Ni		^{60}Ni		^{62}Ni		^{64}Ni		Tuning Rate ^c
			Flux Density ^a	o-c ^b	Flux Density	o-c	Flux Density	o-c	Flux Density	o-c	
F ₁ , J=7/2 ← 5/2, 186.0 μm (1 611 421.9 MHz), CH ₃ OH, Pump 9R(14)											
5/2 ← 5/2	1/2	- ← +	172.72	-0.4	105.12	0.9	41.70	-0.2			-13.1
5/2 ← 5/2	-1/2	- ← +	173.61	-1.2	105.99	-0.9	42.59	-1.9			-13.1
5/2 ← 5/2	1/2	+ ← -	173.61	1.9	105.99	2.9	42.59	2.1			-13.1
5/2 ← 5/2	-1/2	+ ← -	174.48	0.8	106.88	1.3	43.48	0.4			-13.1
3/2 ← 3/2	1/2	- ← +	289.07	-0.2	175.80	-0.2	70.00	-0.0			-7.8
3/2 ← 3/2	-1/2	- ← +	290.22	1.0	176.91	0.7	71.13	1.0			-7.8
3/2 ← 3/2	1/2	+ ← -	290.22	-0.6	176.91	-0.9	71.13	-0.5			-7.8
3/2 ← 3/2	-1/2	+ ← -	291.40	0.8	178.00	-0.2	72.31	0.9			-7.8
1/2 ← 1/2	*	- ← +	902.78	-1.4	540.96	0.5	212.99	-0.9			-2.4
1/2 ← 1/2	*	+ ← -	906.99	-0.7	544.97	1.1	216.93	-0.2			-2.4
-5/2 ← -5/2	1/2	+ ← -							15.98	-0.4	13.1
-5/2 ← -5/2	-1/2	+ ← -							16.81	2.0	13.0
-5/2 ← -5/2	1/2	- ← +							16.81	-1.9	13.1
-5/2 ← -5/2	-1/2	- ← +							17.73	-0.6	13.0
-3/2 ← -3/2	1/2	+ ← -							26.89	0.2	7.8
-3/2 ← -3/2	-1/2	+ ← -							28.02	-0.7	7.8
-3/2 ← -3/2	1/2	- ← +							28.02	0.6	7.8
-3/2 ← -3/2	-1/2	- ← +							29.16	-0.3	7.8
-1/2 ← -1/2	*	+ ← -							81.86	-0.1	2.6
-1/2 ← -1/2	*	- ← +							85.63	-0.5	2.6
3/2 ← 5/2	1/2	- ← +	111.40	-9.6	68.11	1.4					-20.1
3/2 ← 5/2	-1/2	- ← +	112.86	0.6	69.00	0.9					-20.1
3/2 ← 5/2	1/2	+ ← -	111.87	-9.6	68.47	0.1					-20.1
3/2 ← 5/2	-1/2	+ ← -	113.35	1.0	69.47	1.0					-20.1
1/2 ← 3/2	1/2	- ← +	151.39	-0.4	92.08	-0.2					-14.9
1/2 ← 3/2	-1/2	- ← +	152.19	-2.3	93.06	0.6					-14.9
1/2 ← 3/2	1/2	+ ← -	152.19	2.0	93.06	5.0					-14.9
1/2 ← 3/2	-1/2	+ ← -	153.11	2.0	93.67	0.3					-14.9
-1/2 ← 1/2	1/2	- ← +	233.83	0.2	142.18	-0.3	56.53	-0.7			-9.6
-1/2 ← 1/2	-1/2	- ← +	234.74	0.2	143.19	0.8	57.54	0.4			-9.6
-1/2 ← 1/2	1/2	+ ← -	234.74	-0.5	143.19	0.1	57.54	-0.2			-9.6
-1/2 ← 1/2	-1/2	+ ← -	235.74	0.4	144.18	0.9	58.46	-0.0			-9.6
7/2 ← 5/2	1/2	- ← +	377.25	0.6	229.63	-0.1					-6.0
7/2 ← 5/2	-1/2	- ← +	378.65	2.9	231.09	2.5					-6.0
7/2 ← 5/2	1/2	+ ← -	378.65	-0.3	231.09	-0.7					-6.0
7/2 ← 5/2	-1/2	+ ← -	380.15	2.6	232.46	1.4					-6.0
-3/2 ← -1/2	*	- ← +	513.73	-0.9	311.62	-0.4	124.12	-0.3			-4.3
-3/2 ← -1/2	*	+ ← -	516.05	-0.3	313.97	0.4	126.36	0.3			-4.3
-7/2 ← -5/2	1/2	+ ← -							36.50	-7.6	6.0
-7/2 ← -5/2	-1/2	+ ← -							37.28	-4.8	6.0
-7/2 ← -5/2	1/2	- ← +							37.28	-3.0	6.0
-7/2 ← -5/2	-1/2	- ← +							39.16	-6.8	6.0
3/2 ← 1/2	*	+ ← -							48.10	0.2	4.5
3/2 ← 1/2	*	- ← +							50.30	-0.3	4.5
F ₁ , J=7/2 ← 5/2, 183.6 μm (1 632 666.9 MHz), CH ₂ DOH, Pump 9P(10)											
-5/2 ← -5/2	1/2	+ ← -	1447.65	-0.5	1514.92	-1.6	1577.73	-0.3			13.1
-5/2 ← -5/2	-1/2	+ ← -	1448.53	-1.9	1515.80	0.8	1578.74	0.4	1637.80	-2.4	13.1
-5/2 ← -5/2	1/2	- ← +	1448.53	-2.3	1515.80	-3.4	1578.74	-3.8	1637.80	-2.4	13.1

^a Flux density measured in mT.

^b Residuals in the least-squares fit measured in MHz.

^c Tuning rate in MHz/mT, calculated from the parameters in Table IV.

* Proton hyperfine splitting not resolved.

TABLE II—Continued

M_J	M_I	Parity	^{58}Ni		^{60}Ni		^{62}Ni		^{64}Ni		Tuning Rate ^c
			Flux Density ^a	o-c ^b	Flux Density	o-c	Flux Density	o-c	Flux Density	o-c	
-5/2 ← -5/2	-1/2	- ← +	1449.40	0.2	1516.20	5.3	1579.57	-0.8			13.1
-3/2 ← -5/2	1/2	+ ← -	939.85	2.5	983.52	3.0					20.2
-3/2 ← -5/2	-1/2	+ ← -	940.83	2.2	984.55	1.7					20.2
-3/2 ← -5/2	1/2	- ← +	940.28	3.3	983.89	5.0					20.2
-3/2 ← -5/2	-1/2	- ← +	941.24	3.4	984.95	3.0					20.2
-1/2 ← -3/2	1/2	+ ← -	1261.76	1.1	1320.03	1.3					15.2
-1/2 ← -3/2	-1/2	+ ← -	1262.53	3.6	1320.83	3.3			1426.89	-4.7	15.2
-1/2 ← -3/2	1/2	- ← +	1262.53	-1.2	1320.83	-1.5			1426.89	-4.7	15.2
-1/2 ← -3/2	-1/2	- ← +	1263.39	-0.0	1321.62	0.7					15.2
1/2 ← -1/2	1/2	+ ← -	1913.74	-3.7							10.1
1/2 ← -1/2	-1/2	+ ← -	1914.66	-4.5							10.1
1/2 ← -1/2	1/2	- ← +	1914.66	-3.8							10.1
1/2 ← -1/2	-1/2	- ← +	1915.60	-4.8							10.1
F ₁ , J=11/2 ← 9/2, 118.8 μm (2 522 781.6 MHz), CH ₃ OH, Pump 9R(36)											
9/2 ← 9/2	*	- ← +	1249.89	-0.8	1007.39	-0.7	780.94	0.5	568.97	2.3	-5.7
9/2 ← 9/2	*	+ ← -	1260.99	-0.9	1018.60	0.1	792.04	0.7	579.67	0.4	-5.7
7/2 ← 7/2	*	- ← +	1607.95	-0.0	1295.78	-0.4	1004.68	1.8	731.33	0.7	-4.4
7/2 ← 7/2	*	+ ← -	1622.26	0.1	1310.08	-0.2	1018.60	0.5	745.53	0.7	-4.4
5/2 ← 5/2	*	- ← +			1815.90	-0.1	1407.17	0.4	1024.60	1.2	-3.2
5/2 ← 5/2	*	+ ← -			1836.09	0.5	1427.06	0.3	1044.60	1.6	-3.2
3/2 ← 3/2	*	- ← +							1710.45	-0.1	-1.9
3/2 ← 3/2	*	+ ← -							1744.93	2.3	-1.9
7/2 ← 9/2	*	- ← +	782.34	-1.8	631.00	-0.2					-9.1
7/2 ← 9/2	*	+ ← -	789.34	-2.3	637.90	-1.3					-9.1
5/2 ← 7/2	*	- ← +	909.17	0.4	733.13	-0.0	568.47	-0.2			-7.8
5/2 ← 7/2	*	+ ← -	917.27	-0.4	741.13	-1.3	576.28	-2.7			-7.8
3/2 ← 5/2	*	- ← +	1084.19	-2.4	874.66	-0.1	678.31	0.1			-6.6
3/2 ← 5/2	*	+ ← -	1094.39	0.7	884.37	-0.5	687.91	-0.7			-6.6
1/2 ← 3/2	*	- ← +	1343.97	0.2	1084.19	1.2	840.86	1.0			-5.3
1/2 ← 3/2	*	+ ← -	1356.07	-0.4	1096.20	0.5	852.76	0.0			-5.3
-1/2 ← 1/2	*	- ← +	1766.10	-1.4	1425.10	0.5	1105.39	0.4			-4.0
-1/2 ← 1/2	*	+ ← -	1782.22	-1.7	1441.00	-0.2	1121.59	1.3			-4.0
-3/2 ← -1/2	*	- ← +					1613.25	-0.0			-2.8
-3/2 ← -1/2	*	+ ← -					1636.47	-0.8			-2.8
F ₂ , J=5/2 ← 3/2, 256.0 μm (1 170 941.0 MHz), CH ₂ F ₂ , Pump 9P(24)											
-3/2 ← -3/2	1/2	- ← +	608.29	0.5	721.11	0.2					5.8
-3/2 ← -3/2	-1/2	- ← +	611.38	-0.2	724.24	-0.6					5.8
-3/2 ← -3/2	1/2	+ ← -	1203.88	1.4	1315.80	1.3					5.8
-3/2 ← -3/2	-1/2	+ ← -	1207.02	0.7	1318.90	0.7					5.8
-1/2 ← -1/2	*	- ← +	1767.78	0.9							2.1
-1/2 ← -3/2	1/2	- ← +	406.11	0.3	481.76	-1.2					8.7
-1/2 ← -3/2	-1/2	- ← +	409.11	0.1	484.81	-1.8					8.7
1/2 ← -1/2	1/2	- ← +	729.80	-0.5	864.69	-1.7					4.8
1/2 ← -1/2	-1/2	- ← +	732.90	-0.9	867.50	-0.7					4.8
-1/2 ← -3/2	1/2	+ ← -	798.55	0.4	872.94	0.7					8.7
-1/2 ← -3/2	-1/2	+ ← -	801.45	1.0	876.05	-0.5					8.7
1/2 ← -1/2	1/2	+ ← -	1418.10	-0.5	1548.59	0.8					4.9
1/2 ← -1/2	-1/2	+ ← -	1421.15	-0.8	1551.66	0.4					4.9
-5/2 ← -3/2	1/2	- ← +	1209.92	1.1	1434.04	-0.1					2.9
-5/2 ← -3/2	-1/2	- ← +	1212.90	0.5	1437.14	-1.1					2.9
F ₂ , J=7/2 ← 5/2, 183.6 μm (1 632 666.9 MHz), CH ₂ DOH, Pump 9P(10)											
5/2 ← 5/2	1/2	+ ← -	372.76	-0.1	87.53	-1.2					-3.2
5/2 ← 5/2	-1/2	+ ← -	375.91	0.5	90.83	-0.7					-3.2
3/2 ← 3/2	*	+ ← -	624.06	0.7	149.18	0.2					-1.9
1/2 ← 1/2	*	+ ← -	1875.60	0.9	456.96	6.2					-0.6
-5/2 ← -5/2	1/2	- ← +	1774.88	-0.8							3.2
-5/2 ← -5/2	-1/2	- ← +	1778.28	-3.4							3.2

TABLE II *Continued*

M_J	M_I	Parity	^{58}Ni		^{60}Ni		^{62}Ni		^{64}Ni		Tuning Rate ^c
			Flux Density ^a	o-c ^b	Flux Density	o-c	Flux Density	o-c	Flux Density	o-c	
3/2 ← 5/2	1/2	+ ← -	249.25	0.5							-4.8
3/2 ← 5/2	-1/2	+ ← -	252.30	-0.6							-4.8
1/2 ← 3/2	1/2	+ ← -	341.36	1.4	80.00	-0.6					-3.5
1/2 ← 3/2	-1/2	+ ← -	344.68	1.8	83.40	-0.3					-3.5
-1/2 ← 1/2	*	+ ← -	540.41	-0.7	129.19	-0.4					-2.2
7/2 ← 5/2	*	+ ← -	736.10	-0.1	175.79	0.0					-1.6
-3/2 ← -1/2	*	+ ← -			306.05	-0.9					-0.9
-3/2 ← -5/2	1/2	- ← +	1168.37	0.2							4.9
-3/2 ← -5/2	-1/2	- ← +	1171.57	-1.3							4.9
-1/2 ← -3/2	1/2	- ← +	1586.42	0.1	1838.18	0.5					3.6
-1/2 ← -3/2	-1/2	- ← +	1589.57	-0.5	1841.38	-0.3					3.6

The nuclear hyperfine Hamiltonian for a molecule in a Δ state has been discussed by Steimle *et al.* (26). It has the form

$$H_{\text{hfs}} = aI_zL_z + b_F\mathbf{I}\cdot\mathbf{S} + \frac{1}{3}c(3I_zS_z - \mathbf{I}\cdot\mathbf{S}) - \frac{1}{2}d_\Delta(J_+^2I_+S_+ + J_-^2I_-S_-), \quad (3)$$

where a , b_F , and c are the standard Frosch and Foley parameters (33) and d_Δ is a parity-dependent hyperfine interaction for a molecule in a Δ state.

TABLE III

Transitions Observed in the Far-Infrared LMR Spectrum of ^{61}NiH (F_1 , $J = 7/2 \leftarrow 5/2$; 186.0 μm (1 611 421.9 MHz), CH_3OH , Pump 9R(18))

M_J	M_I^a	Parity	Flux Density ^b	o-c ^c	Tuning Rate ^d
3/2 ← 3/2	1/2	- ← +	115.47	-1.3	-7.7
		+ ← -	116.65	-2.1	-7.7
	-1/2	- ← +	125.96	-2.5	-7.7
		+ ← -	127.13	-3.0	-7.7
	-3/2	- ← +	138.10	-2.2	-7.8
		+ ← -	139.27	-2.4	-7.8
1/2 ← 1/2	3/2	- ← +	353.85	-5.3	-2.5
		+ ← -	357.82	-4.7	-2.5
	1/2	- ← +	368.59	1.1	-2.5
		+ ← -	372.45	1.4	-2.5
	-1/2	- ← +	380.01	2.7	-2.5
		+ ← -	383.86	3.0	-2.5
	-3/2	- ← +	388.03	10.1	-2.5
		+ ← -	391.78	10.2	-2.5

^a Nuclear spin quantum number refers to ^{61}NiH ($I=3/2$).

^b Flux density measured in mT.

^c Residuals from the least-squares fit in MHz.

^d Tuning rate in MHz/mT, calculated from the parameters in Table IV.

The Zeeman Hamiltonian is a little more challenging. Attempts to fit the LMR spectrum using the second-order effective Hamiltonian originally derived to describe molecules in ${}^2\Pi$ states (34) and putting $\Lambda = 2$ were not successful. We have therefore developed an effective Zeeman Hamiltonian up to fourth order in perturbation theory; it contains parity-dependent as well as parity-independent terms for a molecule in a ${}^{2S+1}\Delta$ state. For the sake of brevity, we give only the results of these calculations here. We shall describe the derivation and its interpretation in detail in a separate paper. For a molecule in a ${}^{2S+1}\Delta$ state, the Zeeman Hamiltonian is

$$\begin{aligned}
 H_{\text{zeem}} = & (g_L + g_r)\mu_B B_0 L_Z + g_S\mu_B B_0 S_Z - g_r\mu_B B_0 N_Z + \frac{1}{2}g_I\mu_B(B_+S_- + B_-S_+) \\
 & - \frac{1}{2}g_{rD}\mu_B(B_+J_-J_+J_- + B_-J_+J_-J_+) + \frac{1}{2}g_{lD}\mu_B(B_+S_-J_+J_- + B_-S_+J_-J_+) \\
 & - \frac{1}{2}g_{rS}\mu_B(B_+J_-S_+S_- + B_-J_+S_-S_+) + \frac{1}{2}g_{lS}\mu_B(B_+S_-S_+S_- + B_-S_+S_-S_+) \\
 & + \frac{1}{2}g'_{rD}\mu_B(B_+J_+^3 + B_-J_-^3) + \frac{1}{2}g'_{lD}\mu_B(B_+J_+^2S_+ + B_-J_-^2S_-) \\
 & + \frac{1}{2}g'_{rS}\mu_B(B_+J_+S_+^2 + B_-J_-S_-^2) + \frac{1}{2}g'_{lS}\mu_B(B_+S_+^3 + B_-S_-^3), \quad (4)
 \end{aligned}$$

where B_0 is the applied magnetic flux density (along the laboratory-fixed Z axis) and μ_B is the Bohr magneton. The first two terms contain the orbital and spin magnetic effects. The terms in g_r (rotational Zeeman effect) and g_l (anisotropic correction to the electron spin g -factor) contain second-order contributions as described in Ref. (34). The remaining eight terms are all new. The first four of them are parity independent while the remainder are parity dependent and implicitly link only basis states with $\Delta\Lambda = +4$ or -4 (that is, they give a diagonal contribution in a Δ state). The last of these eight terms has zero diagonal elements for a doublet or triplet state whilst the penultimate term has no diagonal terms in a doublet state. Since we are concerned with a doublet state in this paper, we can omit both these terms from further consideration. Furthermore, for a doublet state,

$$\langle S\Sigma | S_+S_- + S_-S_+ | S\Sigma \rangle = 1. \quad (5)$$

Therefore the matrix elements for the term in g_{lS} are indistinguishable from those involving g_l and similarly the matrix elements of the term in g_{rS} are indistinguishable from those which involve g_r . Thus, for a molecule in a ${}^2\Delta$ state, there are 8 independent g -factors rather than 12.

(iii) Representation of the Effective Hamiltonian

The Hund's case (a), parity conserving wavefunctions (34)

$$|\Lambda; S\Sigma; J\Omega M; \pm \rangle = 1/\sqrt{2} \{ |\Lambda; S\Sigma; J\Omega M \rangle \pm (-)^{J-S} | -\Lambda; S - \Sigma; J - \Omega M \rangle \}$$

are not only a convenient choice for a basis set in which to express the effective Hamiltonian but they are also physically appropriate for NiH in its ground state since the spin-orbit splitting is so much larger than the rotational constant, B .

The matrix elements for most of these terms in this basis set are given elsewhere, those of H_{eff} , Eq. (1) in Ref. (31), those the hyperfine Hamiltonian, Eq. (3) in Refs. (26, 35), and the first four terms in the Zeeman Hamiltonian, Eq. (4) in Ref. (34).

The diagonal matrix elements of the remaining four terms in the Zeeman Hamiltonian are

$$\langle \pm; J_{\frac{3}{2}}^3 M_J | H_5 | \pm; J_{\frac{3}{2}}^3 M_J \rangle = -g_{rD} \mu_B B_0 M_J [(J + \frac{1}{2})^2 - 1]^2 / [2J(J + 1)] \quad (6)$$

$$\langle \pm; J_{\frac{5}{2}}^5 M_J | H_5 | \pm; J_{\frac{5}{2}}^5 M_J \rangle = -g_{rD} \mu_B B_0 M_J [(J + \frac{1}{2})^2 - 4]^2 / [2J(J + 1)] \quad (7)$$

$$\langle \pm; J_{\frac{5}{2}}^5 M_J | H_6 | \pm; J_{\frac{3}{2}}^3 M_J \rangle \\ = g_{lD} \mu_B B_0 M_J [(J + \frac{1}{2})^2 - 4]^{1/2} [(J + \frac{1}{2})^2 - 1] / [2J(J + 1)] \quad (8)$$

$$\langle \pm; J_{\frac{3}{2}}^3 M_J | H_7 | \pm; J_{\frac{3}{2}}^3 M_J \rangle = -g_{rS} \mu_B B_0 M_J [(J + \frac{1}{2})^2 - 1] / [2J(J + 1)] \quad (9)$$

$$\langle \pm; J_{\frac{5}{2}}^5 M_J | H_7 | \pm; J_{\frac{5}{2}}^5 M_J \rangle = -g_{rS} \mu_B B_0 M_J [(J + \frac{1}{2})^2 - 4] / [2J(J + 1)] \quad (10)$$

$$\langle \pm; J_{\frac{5}{2}}^5 M_J | H_8 | \pm; J_{\frac{3}{2}}^3 M_J \rangle = g_{lS} \mu_B B_0 M_J [(J + \frac{1}{2})^2 - 4]^{1/2} / [2J(J + 1)] \quad (11)$$

$$\langle \pm; J_{\frac{5}{2}}^5 M_J | H_9 | \pm; J_{\frac{3}{2}}^3 M_J \rangle \\ = \pm (-)^{J-S} g'_{rD} \mu_B B_0 M_J (J + \frac{1}{2}) [(J + \frac{1}{2})^2 - 1] [(J + \frac{1}{2})^2 - 4]^{1/2} / [2J(J + 1)] \quad (12)$$

$$\langle \pm; J_{\frac{3}{2}}^3 M_J | H_{10} | \pm; J_{\frac{3}{2}}^3 M_J \rangle \\ = \pm (-)^{J-S} g'_{lD} \mu_B B_0 M_J (J + \frac{1}{2}) [(J + \frac{1}{2})^2 - 1] / [2J(J + 1)]. \quad (13)$$

In addition, all these terms have matrix elements off-diagonal in J by 1.

(iv) *Least-Squares fit*

The data for all the isotopomers listed in Tables II and III have been fitted with the effective Hamiltonian described above in Eqs. (1), (3), and (4), together with the measurements of the vibration-rotation fundamental band (24), the fine structure transitions for NiH in $v = 0$ (25), and the lambda-doubling intervals for the ${}^2\Delta_{3/2}$ spin component (26). Individual measurements in the mid-infrared, far-infrared, and microwave regions were assigned relative weights of 1, 100, and 10 000, respectively. The basis set was truncated without loss in accuracy at $\Delta J = \pm 1$. Three of the four proton hyperfine parameters were determinable from our data set. We have guessed a value for the Fermi contact parameter, b_F , of -58 MHz from other open shell hydrides (36, 37); the choice does not have a very strong effect on the values for the parameters determined in our fit. Furthermore, two of the g -factors in Eq. (4), g_{rD} and g'_{rD} , were not determinable in practice and so their values were constrained to zero. (The value of the latter can be estimated to be very small from the expression $g'_{rD} = -2q_{\Delta}/B = 4.0 \times 10^{-6} \text{ cm}^{-1}$.) The values determined for the molecular parameters of ${}^{58}\text{NiH}$ are given in Table IV, together with their standard deviations and correlation coefficients. The residuals determined for the far-infrared data are given in Tables II and III. The measurements for the ${}^2\Delta_{5/2}$ component are fitted to within experimental uncertainty while those for the ${}^2\Delta_{3/2}$ component are very nearly so. The vibration-rotation data are fitted slightly better than previously (24), to within experimental error. The microwave measurements of the lambda-doubling intervals are fitted as well as before (26).

TABLE IV

Molecular Parameters for ^{58}NiH in Its $X^2\Delta$ State, Determined in a Least-Squares Fit of Far-Infrared, Mid-Infrared, and Microwave Data

Parameter	Value determined		Correlation coefficient κ_j^a
	MHz	cm^{-1}	
ν_0		1927.684 51 (56) ^{b,c}	84.3
$\omega_e x_e$		39.71 (18) ^c	1.63
B_0	232 429.6 (16)	7.753 016 (55)	10 219
α_e	7 686.8 (23)	0.256 403 (78)	450
D_0	16.620 1 (64)	$5.543 9 (21) \times 10^{-4}$	260
β_e	-0.817 (71)	$-2.73 (24) \times 10^{-5}$	169
A_0	-14 734 346 (258)	-491.484 9 (86)	29 344
γ_0	40 083 (234)	1.337 0 (78)	32 835
γ_D	203.27 (80)	$6.781 (27) \times 10^{-3}$	1 802
$\Delta_{01}(\text{Ni})$		-31.78 (62)	6 785
$\Delta_{0A}(\text{Ni})$		-8.2 (16) ^d	22 479
$\Delta_{0\gamma}(\text{Ni})$		-786 (49)	22 658
$p_{\Delta+4q_{\Delta}}$	188.614 (18)	$6.291 50 (59) \times 10^{-3}$	21.4
$(p_{\Delta+4q_{\Delta}})_D$	0.108 11 (79)	$3.606 (26) \times 10^{-6}$	22.8
q_{Δ}	-0.464 7 (92)	$-1.550 (31) \times 10^{-5}$	1.34
α_q	14.94 (18)	$4.982 (61) \times 10^{-4}$	1.00
$h_{5/2}(\text{H})$	40.0 (13)	$1.334 (43) \times 10^{-3}$	1.32
$h_{3/2}(\text{H})$	51.1 (13)	$1.705 (43) \times 10^{-3}$	1.32
$b(\text{H})$	-81.23 ^e	-2.709×10^{-3} ^e	
$d_{\Delta}(\text{H})$	0.757 (47)	$2.53 (16) \times 10^{-5}$	1.70
$h_{5/2}({}^{61}\text{Ni})$	441.2 (42)	$1.472 (136) \times 10^{-3}$	1.04
$e_{q0}Q({}^{61}\text{Ni})$	42.3 (97)	$1.51 (32) \times 10^{-3}$	1.04
g_L	1.039 759 (40)		3.94
g_S	1.837 08 (16)		4.13
g_r	$-4.019 (10) \times 10^{-2}$		10.2
α_{gr}	$7.34 (17) \times 10^{-3}$		8.63
g_{ℓ}	0.8351 (48)		5.82
$g_{\ell D}$	$1.58 (17) \times 10^{-3}$		5.73
$g_{\ell D'}$	$1.425 (14) \times 10^{-3}$		1.10

^a The correlation parameter $\kappa_j = [\chi^{-1}]_{jj}$ where χ is the matrix of correlation coefficients.

^b The number in parentheses gives the 1 σ error estimate, in units of the last quoted decimal place.

^c ν_0 is the band origin of the (1,0) band for ^{58}NiH . The anharmonicity $\omega_e x_e$ is determined from the variation of ν_0 with Ni isotope.

^d It was necessary to include this parameter in the effective Hamiltonian in order to model the isotopic dependence of the fine structure interval accurately. An equally good fit could be obtained by including α_A in the model instead. Because of the severe perturbations of the ${}^2\Delta_{3/2}$ component in the $v=1$ level, it is difficult to attach any meaning to these parameters. They are better thought of as purely empirical variables.

^e Parameter constrained to this value in the least-squares fit. Value for b_r estimated to be -58 MHz (see text).

5. DISCUSSION

It has proved possible to detect rotational transitions in the NiH radical in both ${}^2\Delta_{5/2}$ and ${}^2\Delta_{3/2}$ spin components by the technique of far-infrared LMR. The experimental measurements for several isotopomers have been satisfactorily modeled with an effective Hamiltonian to yield values for a large number of molecular parameters for ${}^{58}\text{NiH}$. Where comparison is possible, the values obtained agree reasonably well with those determined from the optical spectrum. Kadavathu *et al.* (15) give

$$B_0 = 7.7419(5) \text{ cm}^{-1}, \quad D_0 = 0.540(4) \times 10^{-3} \text{ cm}^{-1}, \quad \text{and } \tilde{\gamma}_0 = 1.89(3) \text{ cm}^{-1}$$

where the last parameter is estimated from the value determined for A_D by use of the relation (38)

$$\tilde{\gamma} = -A_D(A - 2B)\Lambda^2/2B. \quad (14)$$

The observation of lines in the fundamental band of the vibrational spectrum of NiH (24) permits an accurate measurement of the change in the rotational constant with vibrational quantum number. Using the values in Table IV, the equilibrium value for the rotational constant is calculated to be $B_e = 7.881218(67) \text{ cm}^{-1}$, which leads to a value for the bond length r_e for NiH of $0.14694471(62) \text{ nm}$. However, this value is unlikely to be as reliable as implied by the 1σ error estimate because no account has been taken of nonadiabatic mixing. Such effects are known to be severe from studies of the optical spectrum (21). They are also signaled strongly by the values determined in our analysis for the Born-Oppenheimer correction factors $\Delta_{01}(\text{Ni})$ and $\Delta_{07}(\text{Ni})$. From experience with other molecules, these parameters are expected to be negative and have a magnitude between 1 and 10. The values determined are much larger, -31.8 for B_e and -7.86×10^3 for γ_e , presumably because of the heavy mixing with the low-lying ${}^2\Pi$ and ${}^2\Sigma^+$ states.

Three lambda-type doubling parameters have been determined in the fit, the two required for a given vibrational level, $(p_\Delta + 4q_\Delta)$ and q_Δ , and the vibrational dependence of the latter. This third parameter is needed to describe the large lambda doubling observed for the $v = 1$ levels (14, 24). The value for $p_\Delta + 4q_\Delta$ has also been determined from the microwave optical double resonance experiments as $0.0062923(11)$ (26). The present value of $0.00629962(53)$ is very similar because it is primarily determined by the microwave frequencies which were included in our fit.

The authors of the microwave work (26) have shown how the magnitude of $(p_\Delta + 4q_\Delta)$ provides information on the mixing of the low-lying ${}^2\Pi$ and ${}^2\Sigma^+$ states by a fourth-order perturbation calculation. The analogous calculation for q_Δ is even simpler and results in the expression

$$q_\Delta = 2 \langle {}^2\Delta_{5/2} | BL_+ | {}^2\Pi_{3/2} \rangle \langle {}^2\Pi_{3/2} | BL_+ | {}^2\Sigma_{1/2} \rangle \langle {}^2\Sigma_{1/2} | BL_+ | {}^2\Pi_{-1/2} \rangle \\ \times \langle {}^2\Pi_{-1/2} | BL_+ | {}^2\Delta_{-3/2} \rangle / [(E_\Delta - E_\Pi)^2(E_\Delta - E_\Sigma)]. \quad (15)$$

If we approximate the electronic wavefunctions by Ni atomic d orbitals (the pure precession hypothesis)

$$\langle \Lambda \pm 1 | L_\pm | \Lambda \rangle \simeq \langle l, \Lambda \pm 1 | L_\pm | l, \Lambda \rangle = [l(l+1) - \Lambda(\Lambda \pm 1)]^{1/2}, \quad (16)$$

TABLE V

Calculated Rotational Frequencies (in GHz) of NiH in the $X^2\Delta$ State^a

	Transition J F	⁵⁸ NiH	⁶⁰ NiH	⁶² NiH	⁶⁴ NiH		
$^2\Delta_{5/2}$	7/2 ← 5/2	3 ⁺ ← 3 ^{-b}	1613.666	1612.783	1611.956	1611.180	
		3 ⁺ ← 2 ⁻	1613.700	1612.817	1611.989	1611.213	
		4 ⁺ ← 3 ⁻	1613.690	1612.807	1611.980	1611.204	
		3 ⁻ ← 3 ⁺	1613.657	1612.774	1611.947	1611.170	
		3 ⁻ ← 2 ⁺	1613.690	1612.807	1611.980	1611.204	
		4 ⁻ ← 3 ⁺	1613.681	1612.798	1611.970	1611.194	
		9/2 ← 7/2	4 ⁺ ← 4 ⁻	2072.591	2071.458	2070.396	2069.400
		4 ⁺ ← 3 ⁻	2072.615	2071.482	2070.420	2069.424	
		5 ⁺ ← 4 ⁻	2072.609	2071.476	2070.414	2069.418	
		4 ⁻ ← 4 ⁺	2072.619	2071.486	2070.424	2069.428	
		4 ⁻ ← 3 ⁺	2072.643	2071.510	2070.448	2069.452	
		5 ⁻ ← 4 ⁺	2072.637	2071.504	2070.442	2069.446	
	11/2 ← 9/2	5 ⁺ ← 5 ⁻	2529.986	2528.604	2527.310	2526.095	
		5 ⁺ ← 4 ⁻	2530.004	2528.622	2527.328	2526.112	
		6 ⁺ ← 5 ⁻	2530.000	2528.618	2527.324	2526.108	
		5 ⁻ ← 5 ⁺	2529.922	2528.540	2527.246	2526.031	
		5 ⁻ ← 4 ⁺	2529.939	2528.558	2527.263	2526.049	
		6 ⁻ ← 5 ⁺	2529.935	2528.554	2527.259	2526.045	
		$^2\Delta_{3/2}$	5/2 ← 3/2	2 ⁺ ← 2 ⁻	1163.971	1163.324	1162.718
	2 ⁺ ← 1 ⁻			1164.011	1163.364	1162.757	1162.188
	3 ⁺ ← 2 ⁻			1163.996	1163.348	1162.742	1162.172
	2 ⁻ ← 2 ⁺			1167.385	1166.731	1166.120	1165.545
	2 ⁻ ← 1 ⁺			1167.427	1166.773	1166.162	1165.587
	3 ⁻ ← 2 ⁺			1167.415	1166.762	1166.150	1165.576
7/2 ← 5/2	3 ⁺ ← 3 ⁻			1633.841	1632.927	1632.070	1631.267
	3 ⁺ ← 2 ⁻		1633.872	1632.957	1632.101	1631.297	
	4 ⁺ ← 3 ⁻		1633.868	1632.954	1632.097	1631.294	
	3 ⁻ ← 3 ⁺		1626.981	1626.079	1625.233	1624.440	
	3 ⁻ ← 2 ⁺		1627.006	1626.103	1625.257	1624.464	
	4 ⁻ ← 3 ⁺		1626.997	1626.094	1625.249	1624.455	
9/2 ← 7/2	4 ⁺ ← 4 ⁻		2087.831	2086.677	2085.594	2084.580	
	4 ⁺ ← 3 ⁻		2087.847	2086.692	2085.610	2084.595	
	5 ⁺ ← 4 ⁻		2087.840	2086.685	2085.603	2084.588	
	4 ⁻ ← 4 ⁺		2099.3398	2098.164	2097.064	2096.032	
	4 ⁻ ← 3 ⁺		2099.365	2098.191	2097.091	2096.059	
	5 ⁻ ← 4 ⁺		2099.366	2098.191	2097.091	2096.059	

^a Transition frequencies calculated using the parameter values in Table IV.
Accuracy estimated at ± 0.005 GHz.

^b Superscripts refer to the parity of the upper and lower levels.

and $\langle B(r) \rangle$ by B , we obtain

$$q_{\Delta} = 48B^4 / (E_{\Delta} - E_{\Pi})^2 (E_{\Delta} - E_{\Sigma}). \quad (17)$$

We can now calculate a value for q_{Δ} using $B = 7.87 \text{ cm}^{-1}$ and the energy denominators from the optical deperturbation analysis (39), $(E_{\Delta} - E_{\Pi}) = -2193 \text{ cm}^{-1}$ and $(E_{\Delta} - E_{\Sigma}) = -1953 \text{ cm}^{-1}$. The value obtained is $-1.96 \times 10^{-5} \text{ cm}^{-1}$, in good agreement with the experimental value of $-1.550(31) \times 10^{-5} \text{ cm}^{-1}$. The absolute parities of the levels involved in this study have been assigned to be consistent with the calculated signs of the lambda-doubling parameters (26) since they cannot be determined from our experiment.

Three proton hyperfine parameters have been determined for NiH in its $X^2\Delta$ state, out of a possible four. The other hyperfine parameter, b_F , can only be guessed at at this stage but fortunately the results are not greatly affected by the value adopted. The value for the first-order hyperfine parameter for the levels of the $^2\Delta_{3/2}$ spin component, $h_{3/2} = 2a - \frac{1}{2}(b + c)$, is in good agreement with that determined from the microwave study of $50.8 \pm 1.4 \text{ MHz}$. Combination of the values for $h_{3/2}$ and $h_{5/2}$ from Table IV gives

$$\begin{aligned} a &= 0.760(12) \times 10^{-3} \text{ cm}^{-1} & \text{or} & & 22.78 \pm 0.36 \text{ MHz} \\ (b + c) &= -3.71(71) \times 10^{-4} \text{ cm}^{-1} & \text{or} & & -11.1 \pm 2.1 \text{ MHz}. \end{aligned}$$

In other words, $(b + c)$ is only just determined. The value for a , however, can be used to determine the expectation value $\langle 1/r^3 \rangle = 2.89(5) \times 10^{29} \text{ m}^{-3}$, where r is the separation of the open shell electron from the proton in NiH (33). This value is very close to $r_c^{-3} = 3.145 \times 10^{29} \text{ m}^{-3}$ and confirms that the distribution of the open shell electron is indeed well described by an orbital centered on the nickel atom.

Finally, values for six of the eight possible g -factors in the effective Zeeman Hamiltonian, Eq. (4), have been determined. Although the successful fit of the data required all these parameters, the present exercise is not a particularly good test of the new Hamiltonian. We have already seen warning signs that the effective Hamiltonian is finding it difficult to model the rotational energy levels of NiH and there are further indications in the g -factors. Both the orbital and spin g -factors, g_L and g_S , have values considerably different from the free electron values of 1.0 and 2.0023. Furthermore, the rotational g -factor is about two orders of magnitude larger than expected and the anisotropic correction to the electron spin g -factor, g_I , is almost as large as g_S itself. We are forced to the conclusion that we are at the very limit of the applicability of the single state effective Hamiltonian in this problem. We have had a similar experience with the far-infrared LMR spectrum of CoH and an even worse one with that of FeH (27, 40). In the case of FeH in particular, it will be necessary to include the effects of nearby electronic states in the analysis.

In Tables V and VI, we give the calculated zero field frequencies of the rotational and rotation-vibrational transitions studied in this work, for the various isotopic forms of NiH. In view of the remarks made in the previous paragraph, the reliability of the extrapolation to zero magnetic field is not as great as for lighter molecules. We estimate that there is an uncertainty of 5 MHz in the far-infrared frequencies (perhaps even larger for the $^2\Delta_{3/2}$ values) and 30 MHz or 0.001 cm^{-1} in the mid-infrared values.

TABLE VI

Calculated Wavenumbers (in cm^{-1}) of Vibrational–Rotational Transitions in the (1,0) Band of NiH in the $X^2\Delta_{5/2}$ State^a

Transition		⁵⁸ NiH	⁶⁰ NiH	⁶² NiH	⁶⁴ NiH
P(7/2)	+ ← –	1872.0785	1871.5834	1871.1194	1870.6839
	– ← +	1872.0790	1871.5838	1871.1199	1870.6844
P(9/2)	+ ← –	1854.9975	1854.5121	1854.0574	1853.6305
	– ← +	1854.9936	1854.5083	1854.0536	1853.6267
Q(5/2)	+ ← –	1925.9052	1925.3805	1924.8890	1924.4276
	– ← +	1925.9061	1925.3814	1924.8899	1924.4285
Q(7/2)	+ ← –	1924.1337	1923.6105	1923.1204	1922.6603
	– ← +	1924.1281	1923.6049	1923.1148	1922.6548
Q(9/2)	+ ← –	1921.8352	1921.3140	1920.8257	1920.3674
	– ← +	1921.8545	1921.3332	1920.8449	1920.3865
R(5/2)	+ ← –	1977.9603	1977.4077	1976.8900	1976.4040
	– ← +	1977.9552	1977.4026	1976.8849	1976.3989
R(7/2)	+ ← –	1990.9714	1990.4124	1989.8887	1989.3971
	– ← +	1990.9890	1990.4299	1989.9062	1989.4146
R(9/2)	+ ← –	2003.4582	2002.8932	2002.3639	2001.8670
	– ← +	2003.4119	2002.8470	2002.3178	2001.8211

^a Transition wavenumbers calculated using the parameter values in Table IV.

Accuracy estimated at $\pm 0.001 \text{ cm}^{-1}$.

ACKNOWLEDGMENT

We are very grateful to Klaus Lipus, University of Bonn, for providing us with the details of the fine structure transitions and for some help with the computation.

RECEIVED: April 1, 1991

REFERENCES

1. T. M. UPTON, *J. Am. Chem. Soc.* **106**, 1561–1571 (1984).
2. P. E. M. SIEGBAHN, M. R. A. BLOMBERG, I. PANAS, AND U. WAHLGREN, *Theor. Chim. Acta* **75**, 143–159 (1984).
3. D. L. LAMBERT AND E. A. MALLIA, *Mon. Not. R. Astron. Soc.* **151**, 437–447 (1971).
4. M. R. A. BLOMBERG, P. E. M. SIEGBAHN, AND B. O. ROOS, *Mol. Phys.* **47**, 127–143 (1982).
5. S. P. WALCH AND C. W. BAUSCHLICHER, *Chem. Phys. Lett.* **86**, 66–70 (1982).
6. S. P. WALCH AND C. W. BAUSCHLICHER, *J. Chem. Phys.* **78**, 4597–4605 (1983).
7. S. P. WALCH, C. W. BAUSCHLICHER, AND S. R. LANGHOFF, *J. Chem. Phys.* **83**, 5351–5352 (1985).
8. C. M. MARIAN, *J. Chem. Phys.* **93**, 1176–1186 (1990).

9. A. G. GAYDON AND R. W. PEARSE, *Nature (London)* **134**, 287 (1934).
10. A. G. GAYDON AND R. W. PEARSE, *Proc. R. Soc. A* **148**, 312–335 (1935).
11. A. HEIMER, PhD thesis, University of Stockholm, 1937.
12. N. ÅSLUND, H. NEUHAUS, A. LAGERQVIST, AND E. ANDERSON, *Ark. Fys.* **28**, 273–283 (1964).
13. R. E. SMITH, *Proc. R. Soc. London A* **322**, 113–127 (1973).
14. R. SCULLMAN, S. LÖFGREN, AND S. ADAKKAI KADAVATHU, *Phys. Scr.* **25**, 295–301 (1982).
15. S. ADAKKAI KADAVATHU, S. LÖFGREN, AND R. SCULLMAN, *Phys. Scr.* **35**, 277–285 (1987).
16. A. E. STEVENS MILLER, C. S. FEIGERLE, AND W. C. LINEBERGER, *J. Chem. Phys.* **84**, 1549–1556 (1987).
17. J. A. GRAY, S. F. RICE, AND R. W. FIELD, *J. Chem. Phys.* **82**, 4717–4718 (1985).
18. J. A. GRAY AND R. W. FIELD, *J. Chem. Phys.* **84**, 1041–1042 (1986).
19. M. LI, J. A. GRAY, AND R. W. FIELD, *Chem. Phys.* **117**, 171–176 (1987).
20. M. LI AND R. W. FIELD, *J. Chem. Phys.* **90**, 2967–2970 (1989).
21. S. ADAKKAI KADAVATHU, R. SCULLMAN, J. A. GRAY, M. LI, AND R. W. FIELD, *J. Mol. Spectrosc.* **140**, 126–140 (1990).
22. E. J. HILL AND R. W. FIELD, *J. Chem. Phys.* **93**, 1–5 (1990).
23. R. B. WRIGHT, J. K. BATES, AND D. A. GRUEN, *Inorg. Chem.* **17**, 2275–2278 (1978).
24. T. NELIS, E. BACHEM, W. BOHLE, AND W. URBAN, *Mol. Phys.* **64**, 759–765 (1988).
25. K. LIPUS, E. BACHEM, AND W. URBAN, *Mol. Phys.*, submitted.
26. T. C. STEIMLE, D. F. NACHMAN, J. E. SHIRLEY, D. A. FLETCHER, AND J. M. BROWN, *Mol. Phys.* **69**, 923–932 (1990).
27. S. P. BEATON, K. M. EVENSON, T. NELIS, AND J. M. BROWN, *J. Chem. Phys.* **89**, 4446–4448 (1988).
28. T. J. SEARS, P. R. BUNKER, A. R. W. MACKELLAR, K. M. EVENSON, D. A. JENNINGS, AND J. M. BROWN, *J. Chem. Phys.* **77**, 5348–5362 (1982).
29. M. INGUSCIO, G. MORUZZI, K. M. EVENSON, AND D. A. JENNINGS, *J. App. Phys.* **60**, R161–R192 (1986).
30. J. M. BROWN, E. A. COLBOURN, F. D. WAYNE, AND J. K. G. WATSON, *J. Mol. Spectrosc.* **74**, 294–318 (1979).
31. J. M. BROWN, A. S-C. CHEUNG, AND A. J. MERER, *J. Mol. Spectrosc.* **124**, 464–475 (1987).
32. J. K. G. WATSON, *J. Mol. Spectrosc.* **80**, 411–421 (1980).
33. R. A. FROSCHE AND H. M. FOLEY, *Phys. Rev.* **88**, 1337–1349 (1952).
34. J. M. BROWN, M. KAISE, C. M. L. KERR, AND D. J. MILTON, *Mol. Phys.* **36**, 553–582 (1978).
35. A. CARRINGTON, P. N. DYER, AND D. H. LEVY, *J. Chem. Phys.* **47**, 1756–1763 (1967).
36. C. R. BRAZIER AND J. M. BROWN, *Can. J. Phys.* **62**, 1563–1578 (1984).
37. R. J. VAN ZEE, T. C. DEVORE, AND W. WELTNER, *J. Chem. Phys.* **71**, 2051–2056 (1979).
38. J. M. BROWN AND J. K. G. WATSON, *J. Mol. Spectrosc.* **65**, 65–74 (1977).
39. J. A. GRAY, M. LI, T. NELIS, AND R. W. FIELD, to be submitted.
40. S. P. BEATON, K. M. EVENSON, AND J. M. BROWN, to be submitted.